J Inorg Organomet Polym (2015) 25:671–679
DOI 10.1007/s10904-014-0140-y

# Metal(II)-Directed Various Polyoxometalates-Based Hybrid Compounds: Assembly, Structures and Properties

**Xiu-Li Wang · Dan-Na Liu · Hong-Yan Lin · Na Han · Guo-Cheng Liu**

Received: 22 October 2014 / Accepted: 6 December 2014 / Published online: 17 December 2014


**Abstract** Three new polyoxometalates (POMs)-based hybrid compounds: $H_6[Cu(C_5H_5N_2)_2(Mo_8O_{27})(H_2O)_2]\cdot 2(C_5H_6N_2)\cdot 2H_2O$ (**1**), $H_6[Co(C_5H_5N_2)_2(Mo_8O_{27})(H_2O)_2]\cdot 2(C_5H_6N_2)\cdot 2H_2O$ (**2**) and $H_4[(C_5H_6N_2)_2\{Ni(OH)_6Mo_6O_{18}\}]\cdot 4H_2O$ (**3**) ($C_5H_6N_2$ = 3-aminopyridine), have been synthesized by self-assembly of $(NH_4)_6Mo_7O_{24}\cdot 4H_2O$, $C_5H_6N_2$ and different metal nitrates at different pH values. The single crystal X-ray diffraction, IR spectra, PXRD and thermogravimetric analyses have been used to characterize the title compounds. Compounds **1** and **2** are isostructural 3D metal–organic frameworks with a $CdSO_4$-type topology, which are constructed from infinite $Mo_8O_{27}^{6-}$ inorganic chains in uncommon ABAB linking mode. Compound **3** exhibits a 1D supramolecular chain derived from in situ formed Anderson-type $[Ni(OH)_6Mo_6O_{18}]^{4-}$ anions and 3-aminopyridine via hydrogen-bonding interactions. The structural diversities indicate that metal ions show great effect on the construction of different POMs and final architectures. The electrochemical behavior of compound **1**, the photocatalytic activities of compounds **1–3** have been investigated in detail.

**Keywords** Octamolybdate · Anderson-type polyoxometalate · Hybrid compound · Photocatalytic property

**Electronic supplementary material** The online version of this article (doi:10.1007/s10904-014-0140-y) contains supplementary material, which is available to authorized users.

X.-L. Wang (✉) · D.-N. Liu · H.-Y. Lin · N. Han · G.-C. Liu
Department of Chemistry, Liaoning Province Silicon Materials Engineering Technology Research Centre, Bohai University, Jinzhou 121000, People's Republic of China
e-mail: wangxiuli@bhu.edu.cn

## 1 Introduction

The design and construction of polyoxometalate (POMs)-based inorganic–organic hybrid compounds have become the contemporary focus in the fields of inorganic materials and crystal engineering not only due to their diverse structures and unique physical and chemical properties, but also because of their wide range of applications, such as catalysis, electrochemistry, adsorption and photochemistry [1–8]. Many factors including initial reactants and their stoichiometry ratios, nature of organic ligands and metal ions, pH value and temperature can influence the ultimate structures of POMs-based hybrid compounds [9–11]. Of all these factors, the selection of metal ions is of primary importance in the self-assembly process due to the unclear formation mechanism and multiple coordination modes of metal ions [12–14]. For example, Wang's group has successfully obtained four Keggin-based compounds with different structures using different transition metal ions under hydrothermal conditions [15].

In the POMs-based hybrid compounds, the octamolybdate-based compounds represent one of the important branches [16, 17]. The structural diversity and potential coordination capability of octamolybdate polyanions may promote great interest in building high dimensional POMs-based frameworks [18–20]. For example, Ma's group has successfully synthesized two three-dimensional (3D) $Mo_8O_{26}^{4-}$-based compounds $[Ag_{0.52}Na_{0.48}(\beta\text{-}Mo_8O_{26})(H_2O)][Ag_3(Tipa)_2]$ and $[Ag_6(Tipa)_4(\beta\text{-}Mo_8O_{26})][H_2(\beta\text{-}Mo_8O_{26})]\cdot 5H_2O$ with a tri(4-imidazolylphenyl) amine (Tipa) [21]. Wang's group also synthesized two 3D $Mo_8O_{26}^{4-}$-based hybrid compounds: $[Cu^I(bix)][(Cu^I bix)(\delta\text{-}Mo_8O_{26})_{0.5}]$ and $H(Cu^I bix)[(Cu^I bix)_2(\beta\text{-}Mo_8O_{26})]_3\cdot 2H_2O$ (bix = 1,4-Bis(imidazol-1-ylmethyl)benzene) under hydrothermal conditions [22]. However, to our knowledge,

**Table 1** Crystal data and structure refinements for compounds **1–3**

| Formula | $C_{20}H_{36}CuMo_8N_8O_{31}$ | $C_{20}H_{36}CoMo_8N_8O_{31}$ | $C_{10}H_{30}Mo_6N_4NiO_{28}$ |
|---|---|---|---|
| $F_w$ | 1715.63 | 1711.02 | 1288.73 |
| Crystal system | Monoclinic | Monoclinic | Triclinic |
| Space group | C2/c | C2/c | P-1 |
| $a$ (Å) | 20.4469(6) | 20.2455 (9) | 7.8150 (5) |
| $b$ (Å) | 10.2715(3) | 10.3106 (5) | 10.1690 (6) |
| $c$ (Å) | 21.1301(6) | 21.1660 (10) | 10.4940 (7) |
| $\alpha$ (°) | 90 | 90 | 88.0530 (10) |
| $\beta$ (°) | 97.75 | 97.7170 (10) | 77.9580 (10) |
| $\gamma$ (°) | 90 | 90 | 88.9360 (10) |
| $V$ (Å$^3$) | 4,397.2(2) | 4,378.2 (4) | 815.09 (9) |
| $Z$ | 4 | 4 | 1 |
| T (K) | 296(2) | 296 (2) | 296 (2) |
| $D_c$ (g cm$^{-3}$) | 2.592 | 2.596 | 2.625 |
| $F$(000) | 3,300 | 3,292 | 622 |
| Goodness-of-fit on $F^2$ | 1.071 | 1.026 | 1.084 |
| Reflections collected | 10,839 | 12,304 | 4,579 |
| Unique data | 3,864 | 3,860 | 2,860 |
| $R_{int}$ | 0.0124 | 0.0256 | 0.0132 |
| $\theta$ Range (°) | 1.95–25.00 | 1.94–25.00 | 1.99–25.00 |
| $\mu$ (mm$^{-1}$) | 2.783 | 2.688 | 2.907 |
| Final $R_1^a$, $wR_2^b$ [$I > 2\sigma$ ($I$)] | 0.0209, 0.0624 | 0.0253, 0.0680 | 0.0235, 0.0695 |
| Final $R_1^a$, $wR_2^b$ (all data) | 0.0222, 0.0632 | 0.0307, 0.0700 | 0.0248, 0.0666 |
| $\Delta\rho_{max}$ (e Å$^{-3}$) | 0.743 | 1.658 | 0.741 |
| $\Delta\rho_{min}$ (e Å$^{-3}$) | −0.657 | −1.438 | −0.841 |

[a] $R_1 = \Sigma||F_o| - |F_c||/\Sigma|F_o|$

[b] $wR_2 = \Sigma[w(F_o^2 - F_c^2)^2]/\Sigma[w(F_o^2)^2]^{1/2}$

**Scheme. 1** The synthesize processes of compounds **1–3**

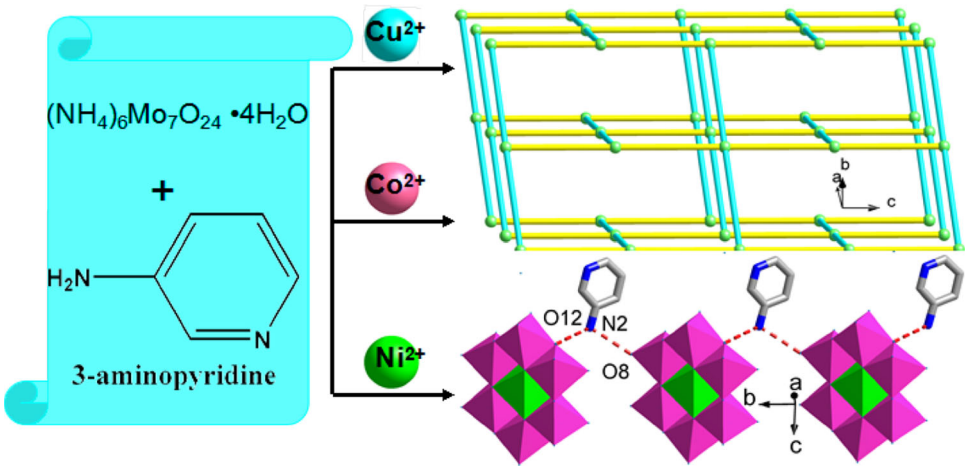


examples of $Mo_8O_{27}^{6-}$-based high dimensional hybrid compounds derived from 1D infinite $Mo_8O_{27}^{6-}$ straight chains by corner-sharing connection are very limited [23–27].

Another important branch in POMs chemistry is Anderson-type POMs-based hybrid compounds [28–30]. Compared to classical Keggin- or Wells–Dawson-type POMs, the reports on combination of Anderson-type POMs and organic motifs are relatively limited, especially those $[Ni(OH)_6Mo_6O_{18}]^{4-}$ ($NiMo_6$)-based inorganic–organic hybrid compounds [31–33]. Up to now, only several examples of $NiMo_6$-based hybrid compounds have been reported [34–37]. For example, Sun's group has reported a $NiMo_6$-based 1D compound $[Himi]_2[Ni(imi)_3(H_2O)\{Ni(OH)_6Mo_6O_{18}\}]\cdot 2H_2O$ (imi = imidazole) [34]. Recently, Xu's group synthesized two $NiMo_6$-based compounds

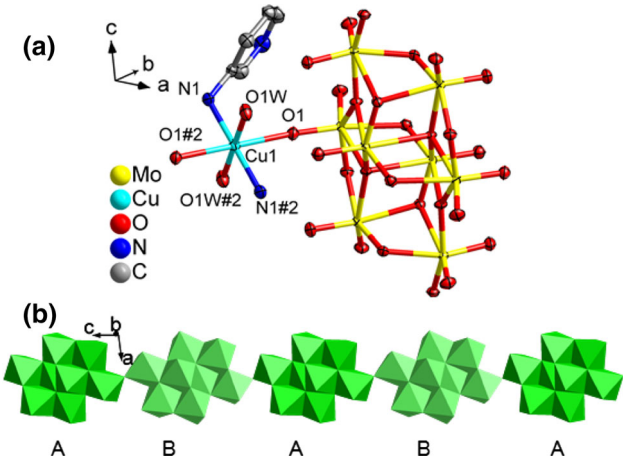


**Fig. 1** **a** The coordination environment of Cu(II) ion in **1** (The hydrogen atoms, discrete water and 3-aminopyridine molecules are omitted for clarity); **b** 1D inorganic $[Mo_8O_{27}]^{6-}$ chains with ABAB mode

$[H_2N(CH_2CH_2)_2O]_4[Na(H_2O)_2\{O(CH_2CH_2)_2NH_2\}]_2[Na(H_2O)_4]_2[V_{10}O_{28}][NiMo_6O_{24}H_6]\cdot 8H_2O$ and $[H_2N(CH_2CH_2)_2O]_6[Na(H_2O)_3]_2[V_{10}O_{28}H_2][NiMo_6O_{24}H_6]\cdot 4H_2O$ [35]. For both examples, all of the $NiMo_6$-based compounds have been prepared by conventional aqueous solution synthesis. Thus, it is significant to further explore a feasible and simple synthesis method of $NiMo_6$-based inorganic–organic hybrid compounds.

In this paper, three new POMs-based hybrid compounds, namely, $H_6[Cu(C_5H_5N_2)_2(Mo_8O_{27})(H_2O)_2]\cdot 2(C_5H_6N_2)\cdot 2H_2O$ (**1**), $H_6[Co(C_5H_5N_2)_2(Mo_8O_{27})(H_2O)_2]\cdot 2(C_5H_6N_2)\cdot 2H_2O$ (**2**) and $H_4[(C_5H_6N_2)_2\{Ni(OH)_6Mo_6O_{18}\}]\cdot 4H_2O$ (**3**) ($C_5H_6N_2$ = 3-aminopyridine ligand) (Scheme 1) have been synthesized by a combination of hydrothermal synthesis and conventional synthesis. The $NiMo_6$ in **3** was in situ synthesized under hydrothermal conditions. Up to now, reports on $Mo_8O_{27}$-based or $NiMo_6$-based hybrid compounds derived from the 3-aminopyridine are scarce. In addition, the electrochemical behavior of compound **1** and the photocatalytic activities of compounds **1**–**3** have been investigated.

## 2 Experimental Section

### 2.1 Materials and Methods

All reagents and solvents for syntheses were purchased from commercial sources and used as received without purification. IR spectra were obtained on Alpha Centaurt FT/IR spectrometer with KBr pellet in the 400–4,000 $cm^{-1}$ region. Thermogravimetric (TG) analyses were recorded on a Pyris-Diamond TG instrument. Electrochemical measurements and data collection were performed with a CHI 440 electrochemical workstation. A conventional three-electrode system was used with a saturated calomel electrode (SCE) as reference electrode and a Pt wire as counter electrode. The compound **1** bulk-modified carbon paste electrode (**1**-CPE) was used as the working electrode. UV–Vis absorption spectra were obtained using a SP-1901 UV–Vis spectrophotometer.

### 2.2 Preparation of the Title Compounds

#### *2.2.1 Synthesis of $H_6[Cu(C_5H_5N_2)_2(Mo_8O_{27})(H_2O)_2]\cdot 2(C_5H_6N_2)\cdot 2H_2O$ (1)*

A mixture of $(NH_4)_6Mo_7O_{24}\cdot 4H_2O$ (0.124 g, 0.1 mmol), $C_5H_6N_2$ (0.0096 g, 0.15 mmol) and $Cu(NO_3)_2\cdot 3H_2O$ (0.12 g, 0.5 mmol) was dissolved in 10 mL distilled water and stirred for 0.5 h at room temperature. The mixture was adjusted to pH $\approx$ 4.3 with 1.0 M HCl, then transferred to a Teflon lined autoclave (25 mL) and kept at 120 °C for 4 days. After slow cooling to room temperature, the blue solution was obtained. The solution was then passed through filter paper to remove the unreacted materials. The filtrate was allowed to stand under ambient conditions for crystallization. Green crystals of **1** were isolated within 12 h in about 52 % yield (based on Cu). IR (KBr, $cm^{-1}$): 3429w, 3348m, 3277m, 2360m, 1616m, 1551s, 1477m, 1384s, 1139m, 924m, 885s, 803w, 677s.

#### *2.2.2 Synthesis of $H_6[Co(C_5H_5N_2)_2(Mo_8O_{27})(H_2O)_2]\cdot 2(C_5H_6N_2)\cdot 2H_2O$ (2)*

The preparation process of compound **2** was similar to that of **1** except that $Co(NO_3)_2\cdot 6H_2O$ (0.14 g, 0.5 mmol) was used instead of $Cu(NO_3)_2\cdot 3H_2O$ (0.12 g, 0.5 mmol). In addition, the pH was adjusted to about 4.1 with 1.0 M HCl. After slow cooling to room temperature, pink solution was obtained. The solution was handled similarly to that of **1**, pink crystals of **2** were isolated within 24 h in about 40 % yield (based on Co). IR (KBr, $cm^{-1}$): 3356m, 3221m, 3046m, 2360,1621m,1560s, 1490m, 1072m, 931s, 887s, 837m, 675m, 622w.

#### *2.2.3 Synthesis of $H_4[(C_5H_6N_2)_2\{Ni(OH)_6Mo_6O_{18}\}]\cdot 4H_2O$ (3)*

Compound **3** was synthesized by the similar procedure used for **1** except that anhydrous $Ni(NO_3)_2$ (0.06 g, 0.5 mmol) was used instead of $Cu(NO_3)_2\cdot 3H_2O$ (0.12 g, 0.5 mmol) and the pH was adjusted to about 4.5 with 1.0 M HCl. Blue-green crystals of **3** were isolated in about 48 % yield within 24 h with the same processing method as above (based on Ni). IR (KBr, $cm^{-1}$): 3403 m, 3325 s,

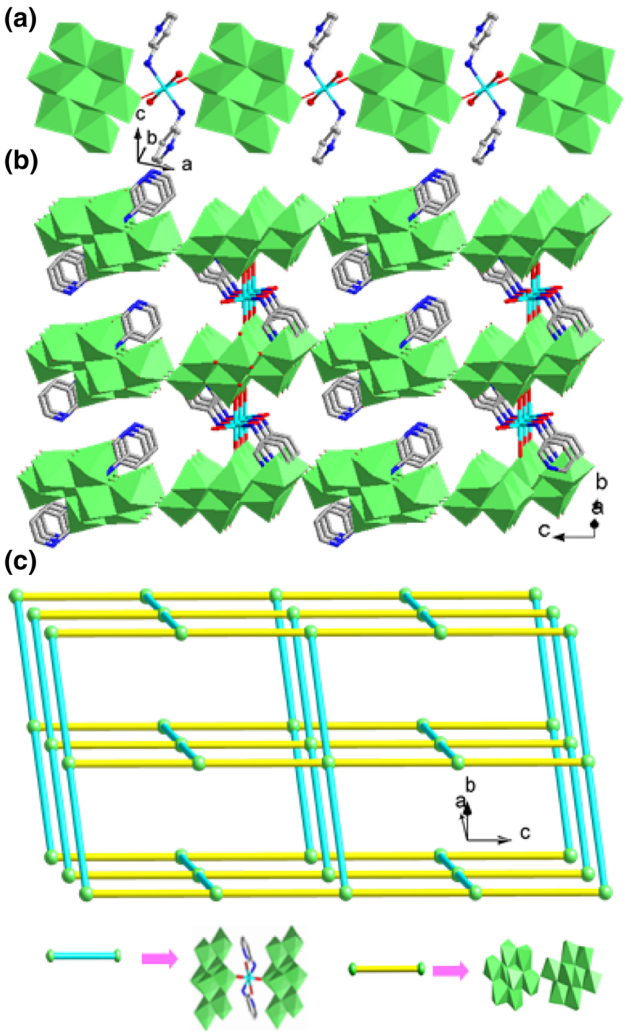


**Fig. 2** **a** The 1D chain connected by $[Cu(C_5H_5N_2)_2(H_2O)_2]$ along *a* axis in **1**; **b** The 3D framework of compound **1** (All discrete 3-aminopyridine and water molecules are omitted for clarity); **c** Schematic view of the 4-connected 3D framework with $CdSO_4$ topology

3207w, 2360 m, 1658 m, 1605w, 1568 s, 1483 m, 1398w, 943 s, 891 s, 661 s, 547 m.

### 2.3 X-Ray Crystallography

Crystallographic data for compounds **1–3** were collected on a Bruker Smart APEX II diffractometer with Kα ($\lambda = 0.71073$ Å) by $\theta$ and $\omega$ scan mode at 296 K. All the structures were solved by direct methods using the SHELXS program of the SHELXTL package and refined on $F^2$ by full-matrix least-squares methods with SHELXL [38]. Anisotropic thermal parameters were used to refine all non-hydrogen atoms. All the hydrogen atoms attached to carbon atoms and nitrogen atoms were fixed in calculated positions, while the hydrogen atoms attached to water molecules were not located but were included in the structure factor calculations. Otherwise, six hydrogen atoms for compounds **1** and **2,** four hydrogen atoms for compound **3** were added to the final formula in order to balance the charge, but were not located. The crystal data and structure refinements for compounds **1–3** were summarized in Table 1. Selected bond lengths (Å) and angles (°) were listed in Table S1–S3. The hydrogen bond parameters of compound **3** are presented in Table S4. Crystallographic data for the structures reported in this paper have been deposited in the Cambridge Crystallographic Data Center with CCDC numbers 1015838, 1015835 and 1015836.

### 2.4 Preparation of 1-CPE

The compound **1** bulk-modified carbon paste electrode (**1**-CPE) was fabricated as follows: 75 mg of graphite powder and 6 mg of **1** were mixed and ground together by an agate mortar and pestle to achieve a uniform mixture, and then 0.1 mL of Nujol was added with stirring. The homogenized mixture was packed into a glass tube with a 1.5 mm inner diameter, and the tube surface was wiped with weighing paper. Electrical contact was established with a copper rod through back of the electrode.

## 3 Results and Discussion

### 3.1 Synthesis

In the process of synthesis, several factors can influence the formation of crystal phases, such as molar ratio, pH value, initial reactants, reaction time, crystallization temperature, filling volume etc. [39–41]. Majority of the POMs-based hybrid compounds are hydrothermally synthesized [26]. However, we have isolated the title compounds by a combination of hydrothermal synthesis and conventional synthesis at room temperature. In this work, lots of parallel experiments showed that pH, crystallization process and reaction temperature were crucial for the formation of title compounds. Such as, for compound **1,** we tried to extend the pH range to pH <4 or pH >4.5, the title products were obtained in lower yield and the crystals were rather poor for X-ray diffraction analysis or nothing could be obtained. In the process of crystallization, the reactant solution was cooled to room temperature with the rate of 7 °C/h, no crystal was obtained. Then the solution was filtrated, and the filtrate was allowed to stand under ambient conditions. After 12–24 h, the corresponding crystals of compounds **1–3** were obtained. Moreover, the crystalline products could be obtained when the reaction temperature was between 110 and 140 °C, however, the highest yield and the best

quality can be observed at the reaction temperature of 120 °C. When the reaction temperature is higher than 140 °C or lower than 110 °C, no crystalline product was obtained after standing the filtrate under ambient conditions more than 1 week.

Besides, metal ions have important influence on the self-assembly process of POMs-based inorganic–organic hybrid compounds. In the synthesis process of the title compounds, when the copper nitrate or cobalt nitrate was used as the initial reactant, two $Mo_8O_{27}$-based 3D metal–organic frameworks **1** and **2** were obtained. However, by using nickel nitrate in the synthesis process of **3**, an Anderson-type $NiMo_6$-based 1D supramolecular chain was synthesized. We also attempted to use other metal nitrates, such as chromium and zinc nitrates, however, the crystals either are too bad to be analyzed by single-crystal X-ray diffraction or can't be obtained. Das's group has isolated five polymolybdate-based hybrid compounds: $[(2\text{-ampH})]_4[\{Zn(H_2O)_5\}Mo_7O_{24}]_3{\cdot}9H_2O$, $[(3\text{-ampH})]_4[\{Zn(3\text{-ampy})(H_2O)_4\}Mo_7O_{24}]_3{\cdot}4H_2O$, $[(3\text{-ampH})]_4[\{Co(3\text{-ampy})(H_2O)_4\}Mo_7O_{24}]_3{\cdot}4H_2O$, $[(2,3\text{-diampH})]_4[Co(H_2O)_6][Mo_7O_{24}]_3{\cdot}6H_2O$ and $[(2,3\text{-diampH})]_2[\{Zn(2,3\text{-diampH})_2(H_2O)_2\}Mo_8O_{27}]_3{\cdot}2H_2O$ (where amp = aminopyridine and diamp = diaminopyridine) in a conventional wet synthesis at room temperature with pH = 2 [26], which further confirmed the significant effect of pH, temperature and initial metal ions on the self-assembly of 3-aminopyridine functionalized polymolybdates.

### 3.2 Structural Description of Compounds 1–3

Single crystal structure analyses reveal that compounds **1** and **2** are isostructural, so only the structure of compound **1** will be described in detail. Compound **1** consists of one $Cu^{II}$ ion, one $[Mo_8O_{27}]^{6-}$ anion, two $[C_5H_5N_2]^-$ anions and two $[C_5H_6N_2]$ molecules. Six hydrogen atoms were added to the final formula in order to balance the charge. The $Cu^{II}$ ion is six-coordinated by two N atoms from two $[C_5H_5N_2]^-$ ligands, two O atoms from two $[Mo_8O_{27}]^{6-}$ polyoxoanions, and two O atoms from two coordinated water molecules, completing a distorted octahedral geometry (Fig. 1a). The bond distances and angles are 2.031(3) Å for Cu–N, 2.021(3)–2.265(2) Å for Cu–O, 88.09(10)–180.00° for O–Cu–O and 85.85(11)–94.15(11)° for O–Cu–N. The $[Mo_8O_{27}]^{6-}$ is the well-known centrosymetric octamolybdate consisting of eight edge-sharing molybdenum-oxygen octahedra. Interestingly, as shown in Fig. 1b, the $[Mo_8O_{27}]^{6-}$ anions exhibit two different orientations and are linked by terminal O atoms into infinite chain in an ABAB mode, which hasn't been observed up to now.

It is noted that each $[Mo_8O_{27}]^{6-}$ anion from the 1D inorganic chain provides two terminal O atoms to coordinate with the $Cu^{II}$ ions of $[Cu(C_5H_5N_2)_2(H_2O)_2]$ subunits (Fig. 2a). Thus, 1D $[Mo_8O_{27}]^{6-}$-based inorganic chains are connected by $[Cu(C_5H_5N_2)_2(H_2O)_2]$ subunits along *a* axis and *b* axis to construct a 3D framework (Fig. 2b). The 3-aminopyridine hanging on both sides of copper ions as terminal ligand has no effect on the dimensionality.

Topologically, if the 3-aminopyridine ligands are ignored, the $[Mo_8O_{27}]^{6-}$ anion linking two $Cu^{II}$ ions and two $[Mo_8O_{27}]^{6-}$ anions is considered as a four-connected node, $[Cu(C_5H_5N_2)_2(H_2O)_2]$ subunits are viewed as linkers, then the whole 3D framework of **1** can be simplified as a 4-connected 3D net with the $CdSO_4$-type topology (Fig. 2c). To our knowledge, compounds **1** and **2** represent the rare high dimensional POMs-based hybrid compounds constructed from $[Mo_8O_{27}]^{6-}$ chains in ABAB mode so far [23–27].

The single-crystal X-ray diffraction analysis reveals that compound **3** consists of an Anderson anion $[Ni(OH)_6Mo_6O_{18}]^{4-}$ ($NiMo_6$), two $C_5H_6N_2$ molecules and four lattice water molecules. Four hydrogen atoms were added to the final formula in order to balance the charge. The $NiMo_6$ is in situ synthesized at the presence of $Ni^{II}$ ion, which shows a typical Anderson structure and consists of seven edge-sharing octahedra, six of which are Mo centered octahedra arranged hexagonally around the central $Ni^{II}(OH)_6$ octahedron (Fig. 3a). The bond distances and angles around $Ni^{II}$ ion are 2.036(2)–2.056(3) Å for Ni–O and 81.04 (10)–180° for O–Ni–O. The Anderson-type $NiMo_6$ anions and 3-aminopyridine molecules are linked via hydrogen-bonding interactions [N(2)-H(2B)···O(8) = 2.17 Å] and [N(2)-H(2A)···O(12) = 2.19 Å] to construct a 1D supramolecular chain (Fig. 3b).

As described above, when $Cu^{II}$ and $Co^{II}$ nitrates were used as the reactants, the octamolybdate polyoxoanion was formed and finally a 3D $CdSO_4$-type framework was constructed. However, when $Ni^{II}$ nitrate was used as the reactant, the Anderson-type polyoxoanion $NiMo_6$ was formed and finally a 1D supramolecular chain was obtained. The results indicate that transition metals show great effect on the formation of polyoxoanions and the final architectures.

### 3.3 IR Spectra of Compounds 1–3

The IR spectra of compounds **1**–**3** are shown in Fig. S1. The characteristic bands at 924, 885, 803 and 677 $cm^{-1}$ for **1**, 931, 887, 837 and 675 $cm^{-1}$ for **2**, and 943, 891, 661, 547 $cm^{-1}$ for **3** are attributed to the $\nu$(Mo = O) and $\nu$(Mo–O–Mo), respectively [19, 34]. The bands observed in the region of 1616, 1551, 1477 $cm^{-1}$ for **1**, 1621, 1560, 1490 $cm^{-1}$ for **2**, 1658, 1605, 1568, 1483 $cm^{-1}$ for **3** are due to the characteristic peaks of 3-aminopyridine [42]. The bands around 3,400 $cm^{-1}$ are ascribed to the water molecules.

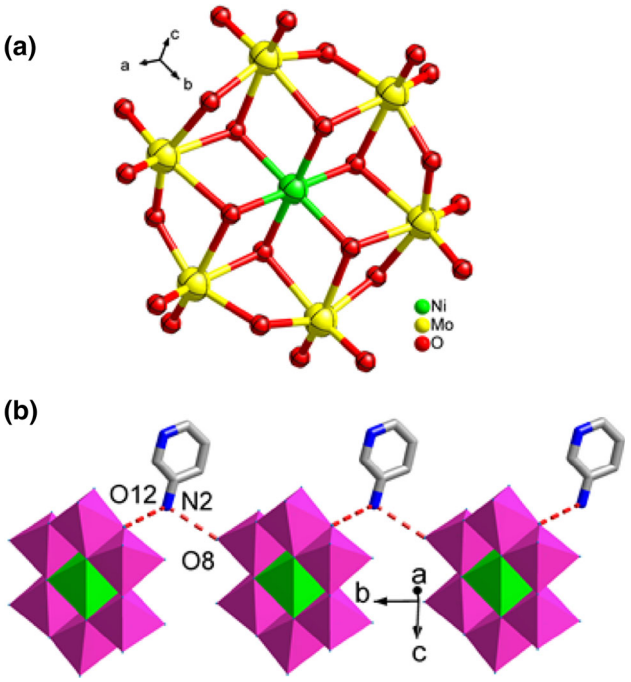


**Fig. 3** **a** The ball/stick representation of $NiMo_6$ anion in compound **3**; **b** The 1D supramolecular chain based on $NiMo_6$ and 3-aminopyridine linked by hydrogen bonding interactions in **3**

### 3.4 Powder X-Ray Diffraction and Thermal Analysis of Compounds 1–3

The PXRD patterns of the synthesized compounds match well with the simulated ones except for some intensity differences (Fig. S2), which can be owed to the different orientation of the crystals in the powder samples, indicating the crystalline phase purity [43].

The TG experiments were performed under $N_2$ atmosphere with a heating rate of 10 °C $min^{-1}$ in the temperature range of 20–800 °C, as shown in Fig. S3. The TG curves of compounds **1**–**3** show three distinct weight loss steps: The first weight loss step below 200 °C for **1** and **2**, 150 °C for **3**, corresponds to the loss of water molecules 4.20 % (calcd. 4.21 %) for **1**, 4.34 % (calcd. 4.22 %) for **2**, 5.78 % (calcd. 5.60 %) for **3**. The second weight loss step corresponds to the loss of organic molecules 11.24 % (calcd. 11.73 %) for **1**, 11.46 % (calcd. 11.76 %) for **2**, 15.15 % (calcd. 15.60 %) for **3**. The third sharp weight loss step starts at 300 °C for **1**, **2** and **3**, which are attributed to collapse of the frameworks.

### 3.5 Electrochemical Properties

The bulk-modified carbon paste electrode (CPE) with the title compounds is the optimal choice to study the electrochemical properties for these compounds, which is due to their insolubilities in water and common organic

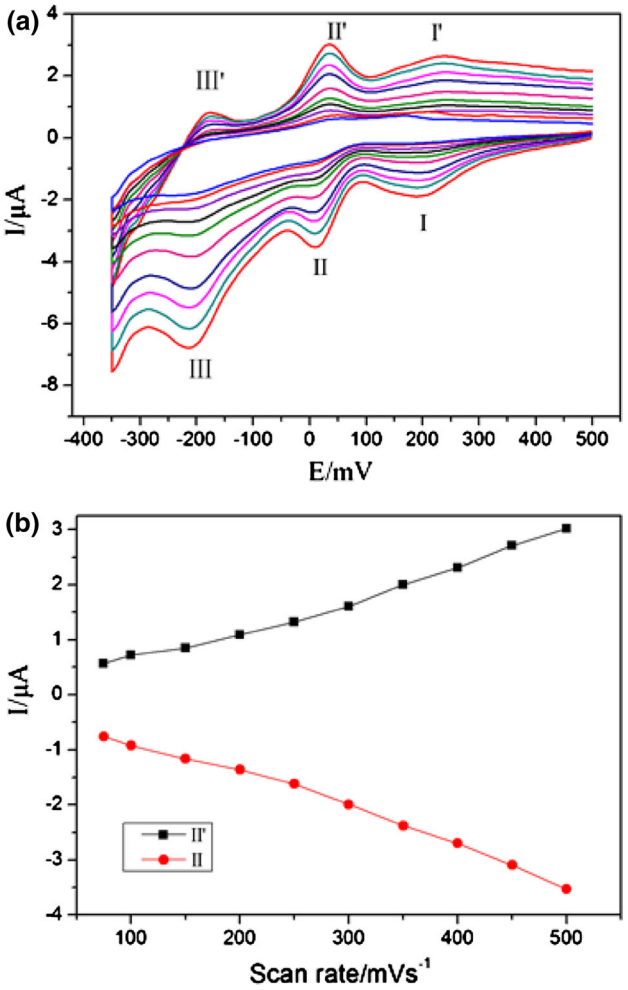


**Fig. 4** **a** Cyclic voltammograms of the **1**-CPE and in 0.1 M $H_2SO_4$ + 0.5 M $Na_2SO_4$ aqueous solution at different scan rates (from inner to outer: 75, 100, 150, 200, 250, 300, 350, 400, 450 and 500 mV $s^{-1}$); **b** Plots of the anodic and cathodic peak II–II′ currents against scan rates

solvents. The electrochemical behaviors of compounds **1** and **2** are similar except for some light potential shift, so compound **1** was taken as an example to study their electrochemical properties. The cyclic voltammograms for **1**-CPE in 0.1 M $H_2SO_4$ + 0.5 M $Na_2SO_4$ aqueous solution at different scan rates in the potential range of −350 to 500 mV are shown in Fig. 4a. Three pairs of reversible redox peaks appear and the mean peak potentials $E_{1/2} = (E_{pa} + E_{pc})/2$ are +218.7 (I–I′), −24.7 (II–II′) and −191.6 (III–III′) mV (scan rate: 200 mV $s^{-1}$), respectively. The redox peaks I–I', II–II' and III–III' should be attributed to three consecutive two-electron redox processes of Mo centers [44, 45]. The peak potentials change gradually following scan rates from 75 to 500 mV $s^{-1}$: the cathodic peak potentials shift towards negative direction and the corresponding anodic peak potentials to positive direction with increasing scan rates (Fig. 4b). When the

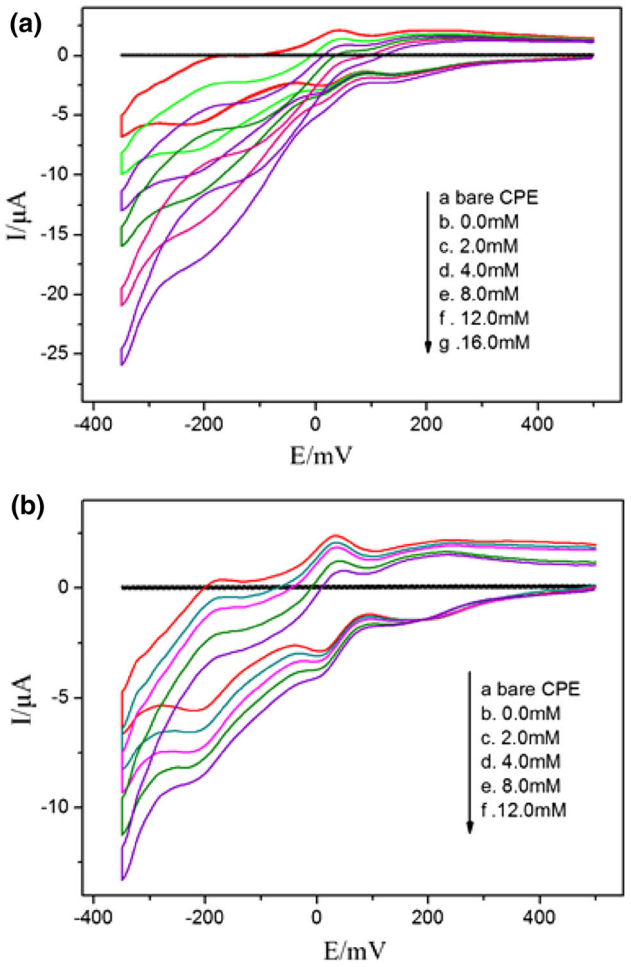


**Fig. 5** Cyclic voltammograms of **1**-CPE in 0.1 M $H_2SO_4$ + 0.5 M $Na_2SO_4$ solution containing 0.0–16.0 mM $KBrO_3$ (**a**) and 0.0–12.0 mM $H_2O_2$ (**b**) Scan rate: 300 mV $s^{-1}$

scan rates are lower than 500 mV $s^{-1}$, the peak currents are proportional to the scan rates, which indicate that the redox process of **1**–CPE is surface-confined [45].

It is well known that some POMs can electrocatalyze reduction of certain substance, such as bromate and hydrogen peroxide. In this paper, **1**-CPE also shows good electrocatalytic activity toward the reduction of bromate and hydrogen peroxide. As can be seen from Fig. 5, at **1**-CPE, with the addition of bromate or hydrogen peroxide, both the reduction peak currents increase gradually and the corresponding oxidation peak currents decrease, suggesting that the reduction of bromate and hydrogen peroxide is electrocatalyzed by the reduced species of $Mo_8O_{27}$ in compound **1**.

### 3.6 Photocatalytic Activity

As is known, POMs often show photocatalytic activity in the degradation of some organic dyes by oxidation of organic materials [46–48]. Ma's group has reported a $Mo_8O_{26}$-based compound $[Ag_8(L_1)_4(\alpha\text{-}Mo_8O_{26})(\beta\text{-}Mo_8O_{26})\text{-}(H_2O)_3]\cdot H_2O$ ($L_1$ = 1,1′-(1,3-propanediyl)-bis[2-(4-pyridyl)benzimidazole]), whose photocatalytic activity can reach 75 % for methylene blue (MB) under UV irradiation [49]. Herein, we also selected MB as a model pollutant in aqueous media to evaluate the photocatalytic effectiveness of compounds **1**–**3**. The photocatalytic performances for MB are investigated through a typical process: 150 mg of samples was dispersed in the MB solution, which was then exposed to UV or sunlight irradiation, and kept continuous stirring. The sample of the MB solution was taken out at regular intervals for analysis.

Firstly, we investigated the photocatalytic performance of the title complexes for the photodegradation of MB under UV light irradiation from a 125 W Hg lamp. MB was almost fully degraded within 25, 25 and 5 min for compounds **1**, **2** and **3**, respectively (Fig. S5). The excellent photocatalytic activity has seldom been observed for POMs-based compounds. So we further performed the photocatalytic tests of the title compounds towards the degradation of MB under sunlight irradiation. As shown in Fig. 6a, b the absorption peaks of MB decreased obviously with increasing reaction time for compounds **1** and **2** under sunlight irradiation. The calculation results show that approximately 78.4 and 82.3 % of MB were decomposed during 150 min for compounds **1** and **2**, respectively. As shown in Fig. 6c, the absorption peak of MB decreased greatly with increasing reaction time for compound **3** under sunlight irradiation. The calculation results show that approximately 85.1 % of MB has been decomposed under sunlight during 35 min. The results indicate that compounds **1**–**3**, especially **3**, exhibit remarkable photocatalytic activities for the degradation of MB under UV and sunlight irradiation. The title compounds may be excellent potential candidates as photocatalytic materials.

## 4 Conclusion

In this paper, three new POM-based hybrid compounds **1**–**3** based on various in situ synthesized polyoxoanions and 3-aminopyridine have been synthesized. Compounds **1** and **2** are isostructural 3D $CdSO_4$-type frameworks constructed from infinite $Mo_8O_{27}$ chains in ABAB mode. Compound **3** is a 1D supramolecular chain derived from in situ formed Anderson-type $NiMo_6$ anions and 3-aminopyridine. The metal ions play an important role in the assembly and structures of the title compounds, especially in the construction of different type of POMs. Compound **1** exhibits good electrocatalytic activities toward the reduction of $KBrO_3$ and $H_2O_2$. The compounds **1**–**3** exhibit remarkable photocatalytic activities for the degradation of MB under

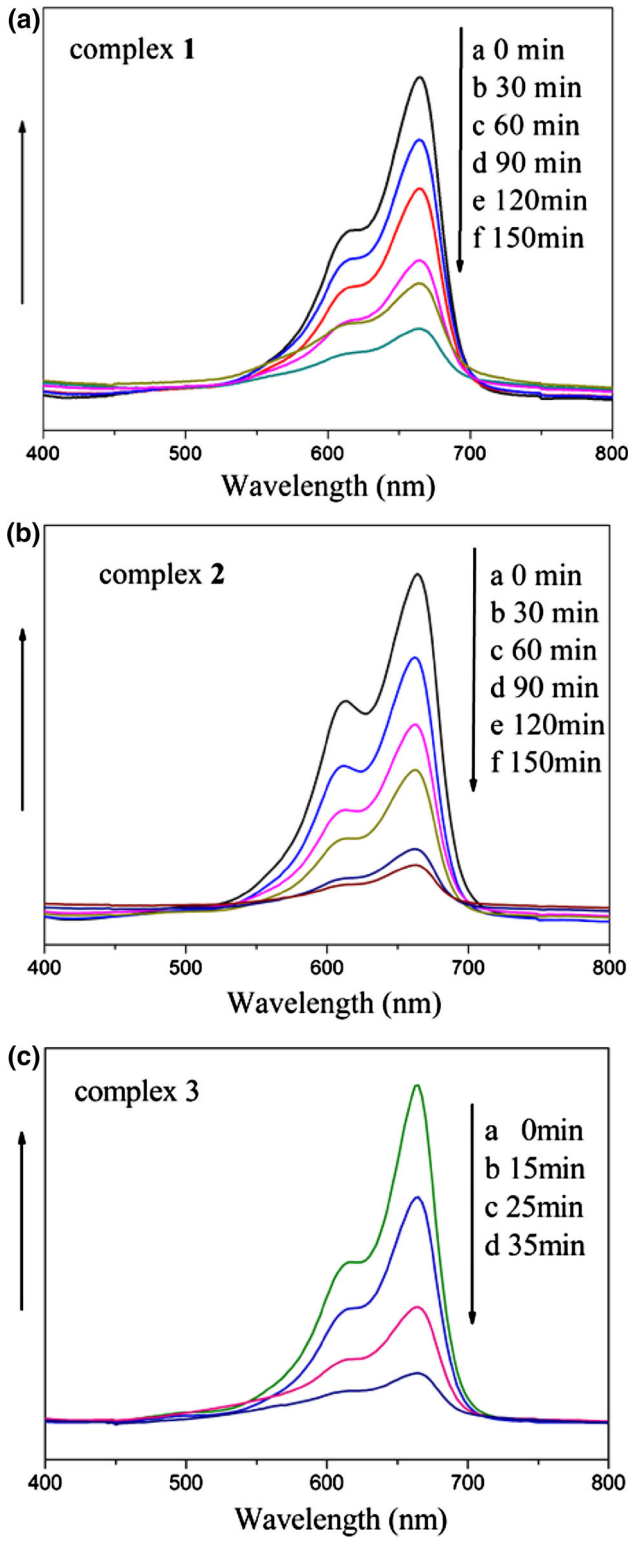


**Fig. 6** Absorption spectra of the MB solution during decomposition reaction under sunlight irradiation at the presence of compound **1** (**a**), **2** (**b**) and **3** (**c**)

UV and sunlight irradiation. These preliminary results display that the title compounds may be potential candidates for electrochemical and photocatalytic materials.

## 5 Supporting Information

X-ray crystallographic files for compounds **1–3** in CIF format. Table of selected bond lengths and angles of compounds **1–3**; Table of selected hydrogen–bonding geometries of compound **3**; IR spectra, PXRD and TGA curves for compounds **1–3**; The photocatalytic degradation curves of compound **1–3** under UV irradiation.

**Acknowledgments** This work was financially supported by the National Natural Science Foundation of China (No. 21171025 and 21471021), Program of New Century Excellent Talents in University (NCET-09-0853), and Program of Innovative Research Team in University of Liaoning Province (LT2012020).

## References

1. B.S. Bassil, M. Ibrahim, R. Al-Oweini, M. Asano, Z.X. Wang, J. Tol, N.S. Dalal, K.-Y. Choi, R.N. Biboum, B. Keita, L. Nadjo, U. Kortz, Angew. Chem. Int. Ed. **50**, 5961 (2011)
2. X.L. Wang, N. Han, H.Y. Lin, A.X. Tian, G.C. Liu, J.W. Zhang, Dalton Trans. **43**, 2052 (2014)
3. M. Singh, S.E. Lofland, K.V. Ramanujachary, A. Ramanan, Cryst. Growth Des. **10**, 5105 (2010)
4. X.J. Kuang, I.R. Evans, Inorg. Chem. **49**, 6005 (2010)
5. W.W. He, S.L. Li, H.Y. Zang, G.S. Yang, S.R. Zhang, Z.M. Su, Y.Q. Lan, Coord. Chem. Rev. **279**, 141 (2014)
6. X.L. Wang, N. Li, A.X. Tian, J. Ying, T.J. Li, X.L. Lin, J. Luan, Y. Yang, Inorg. Chem. **53**, 7118 (2014)
7. F.J. Ma, S.X. Liu, C.Y. Sun, D.D. Liang, G.J. Ren, F. Wei, Y.G. Chen, Z.M. Su, J. Am. Chem. Soc. **133**, 4178 (2011)
8. Y. Gong, T. Wu, P.G. Jiang, J.H. Lin, Y.X. Yang, Inorg. Chem. **52**, 777 (2013)
9. H.Y. An, Y.G. Li, D.R. Xiao, E.B. Wang, C.Y. Sun, Cryst. Growth Des. **6**, 1107 (2006)
10. A. Iturrospe, B. Artetxe, S. Reinoso, L.S. Felices, P. Vitoria, L. Lezama, J.M. Gutiérrez-Zorrilla, Inorg. Chem. **52**, 3084 (2013)
11. A.X. Tian, Y. Yang, N. Sun, J. Ying, X.L. Wang, J. Coord. Chem. **67**, 1550 (2014)
12. Z.F. Chen, H.Y. An, H. Zhang, Y. Hu, CrystEngComm. **15**, 4711 (2013)
13. S.L. Li, Y.Q. Lan, J.F. Ma, J. Yang, X.H. Wang, Z.M. Su, Inorg. Chem. **46**, 8283 (2007)
14. R. Belghiche, O. Bechiri, M. Abbessi, S. Golhen, Y.L. Gal, L. Ouahab, Inorg. Chem. **48**, 6026 (2009)
15. Y. Ding, J.X. Meng, W.L. Chen, E.B. Wang, CrystEngComm. **13**, 2687 (2011)
16. A.X. Tian, X.L. Lin, G.Y. Liu, R. Xiao, J. Ying, X.L. Wang, J. Coord. Chem. **66**, 1340 (2013)
17. L. Luo, H.S. Lin, L. Li, T.I. Smirnova, P.A. Maggard, Inorg. Chem. **53**, 3464 (2014)
18. D.D. Zhang, J. Zhao, Y.H. Zhang, X.J. Hu, L.S. Li, P.T. Ma, J.P. Wang, J.Y. Niu, Dalton Trans. **42**, 2696 (2013)
19. Y.Q. Lan, S.L. Li, X.L. Wang, K.Z. Shao, D.Y. Du, H.Y. Zang, Z.M. Su, Inorg. Chem. **47**, 8179 (2008)
20. W.Q. Kan, J. Yang, Y.Y. Liu, J.F. Ma, Inorg. Chem. **51**, 11266 (2012)
21. H. Wu, J. Yang, Y.Y. Liu, J.F. Ma, Cryst. Growth Des. **12**, 2272 (2012)
22. J.X. Meng, Y. Lu, Y.G. Li, H. Fu, E.B. Wang, Cryst. Growth Des. **9**, 4116 (2009)

23. V. Coué, R. Dessapt, M. Bujoli-Doeuff, M. Evain, S. Jobic, Inorg. Chem. **46**, 2824 (2007)
24. R. Dessapt, M. Collet, V. Coué, M. Bujoli-Doeuff, S. Jobic, C. Lee, M.H. Whangbo, Inorg. Chem. **48**, 574 (2009)
25. D.J. Hubbard, A.R. Johnston, H.S. Casalongue, A.N. Sarjeantand Alexander, J. Norquist, Inorg. Chem. **47**, 8518 (2008)
26. T. Arumuganathan, A.S. Rao, S.K. Das, Cryst. Growth Des. **10**, 4272 (2010)
27. R. Dessapt, M. Gabard, M. Bujoli-Doeuff, P. Deniard, S. Jobic, Inorg. Chem. **50**, 8790 (2011)
28. Y. Hu, H.Y. An, X. Liu, J.Q. Yin, H.L. Wang, H. Zhang, L. Wang, Dalton Trans. **43**, 2488 (2014)
29. J.W. Zhang, Y.C. Huang, J. Zhang, S. She, J. Hao, Y.G. Wei, Dalton Trans. **43**, 2722 (2014)
30. H.Y. An, X. Liu, H. Chen, Z.B. Han, H. Zhang, Z.F. Chen, CrystEngComm. **13**, 5384 (2011)
31. S.Z. Li, P.T. Ma, J.P. Wang, Y.Y. Guo, H.Z. Niu, J.W. Zhao, J.Y. Niu, CrystEngComm. **12**, 1718 (2010)
32. H.Y. An, T.Q. Xu, C.Y. Jia, H. Zheng, W.S. Mu, J. Mol. Struct. **933**, 86 (2009)
33. C. Allain, S. Favette, L.M. Chamoreau, J. Vaissermann, L. Ruhlmann, B. Hasenknopf, Eur. J. Inorg. Chem. **2008**, 3433 (2008)
34. J. Li, L.C. Zhang, Z.G. Sun, C.H. Tian, Z.M. Zhu, Y. Zhao, Y.Y. Zhu, J. Zhang, N. Zhang, L. Liu, X. Lu, Z. Anorg, Allg. Chem. **634**, 1173 (2008)
35. Y.Y. Yang, L. Xu, F.Y. Li, X.S. Qu, Inorg. Chem. Commun. **33**, 142 (2013)
36. B. Hasenknopf, R. Delmont, P. Herson, P. Gouzerh, Eur. J. Inorg. Chem. **2002**, 1081 (2002)
37. H. Liu, L. Xu, Acta Cryst. **E63**, m872 (2007)
38. A.X. Tian, J. Ying, J. Peng, J.Q. Sha, H.J. Pang, P.P. Zhang, Y. Chen, M. Zhu, Z.M. Su, Cryst. Growth Des. **8**, 3717 (2008)
39. J.Q. Sha, J. Peng, Y.Q. Lan, Z.M. Su, H.J. Pang, A.X. Tian, P.P. Zhang, M. Zhu, Inorg. Chem. **47**, 5145 (2008)
40. A.X. Tian, Z.G. Han, J. Peng, J.Q. Sha, Y.L. Zhao, H.J. Pang, P.P. Zhang, M. Zhu, Solid State Sci. **10**, 1352 (2008)
41. A.X. Tian, J. Ying, J. Peng, J.Q. Sha, H.J. Pang, P.P. Zhang, Y. Chen, M. Zhu, Z.M. Su, Inorg. Chem. **48**, 100 (2009)
42. Q. Deng, Y.L. Huang, Z.S. Peng, Z.J. Dai, M.R. Lin, T.J. Cai, J. Solid State Chem. **200**, 60 (2013)
43. B.X. Dong, Q. Xu, Inorg. Chem. **48**, 5861 (2009)
44. X.D. Du, C.H. Li, Y. Zhang, S. Liu, Y. Ma, X.Z. You, CrystEngComm. **13**, 2350 (2011)
45. X.L. Wang, C. Xu, H.Y. Lin, G.C. Liu, J. Luan, Z.H. Chang, RSC. Adv. **3**, 3592 (2013)
46. Y.H. Guo, C.W. Hu, X.L. Wang, Y.H. Wang, E.B. Wang, Chem. Mater. **13**, 4058 (2001)
47. X.L. Wang, C. Xu, H.Y. Lin, G.C. Liu, S. Yang, Q. Gao, A.X. Tian, CrystEngComm. **14**, 5836 (2012)
48. A. Dolbecq, P. Mialane, B. Keita, L. Nadjo, J. Mater. Chem. **22**, 24509 (2012)
49. H.Y. Liu, L. Bo, J. Yang, Y.Y. Liu, J.F. Ma, H. Wu, Dalton Trans. **40**, 9782 (2011)